IEEE Access
Multidisciplinary | Rapid Review | Open Access Journal

Received 27 January 2023, accepted 12 February 2023, date of publication 14 February 2023, date of current version 17 February 2023.

Digital Object Identifier 10.1109/ACCESS.2023.3245065

RESEARCH ARTICLE

Fixed-Time Output Feedback Distributed Cooperative Event-Triggered Control for Multiple Surface Vessels With Prescribed Performance Constraints

ZHEDA REN[1] AND TIAN XIA[2]
[1]College of Intelligent Systems Science and Engineering, Harbin Engineering University, Harbin 150001, China
[2]Shanghai Shipbuilding Technology Research Institute, Shanghai 200032, China

Corresponding author: Zheda Ren (renzheda@hrbeu.edu.cn)

This work was supported in part by the Seventh Generation Ultra Deep Water Drilling Unit Innovation Project.

ABSTRACT This paper studies the distributed cooperative control problem for multiple surface vessels (MSVs) subject to unknown environmental disturbances, model uncertainties, unavailable velocities and prescribed performance constraints. Firstly, a fixed-time extended state observer (FxESO) is designed to provide the estimations of velocities and lumped disturbances (including unknown environmental disturbances and model uncertainties). Secondly, to improve the convergence performance of the MSVs, a hyperbolic cosecant prescribed performance function is incorporated into the cooperative control algorithm. Thirdly, a fixed-time event-triggered control law with prescribed performance constraint is applied to cooperative control based on a fixed-time nonsingular terminal sliding mode manifold (FxNTSMM), and the cooperative errors can converge within fixed time. Finally, by employing Lyapunov function theory, the stability of the closed-loop system is analyzed. Simulation results are given to demonstrate the effectiveness of the proposed control scheme.

INDEX TERMS Multiple surface vessels, fixed-time extended state observer, prescribed performance, fixed-time sliding mode control, event-triggered controller.

I. INTRODUCTION

With the increasingly fierce competition for marine resources in economy, military and other fields, the cooperative control technology of MSVs has developed rapidly [1], [2]. Due to the advantages of wide operating range, high efficiency and satisfactory robustness, cooperative control for MSVs is widely used in replenishment, ocean exploration and maritime patrol [3].

It is necessary to strictly ensure the tracking accuracy and convergence rate of cooperative control for MSVs to avoid a series of losses as some urgent missions need to reach the predetermined position quickly and accurately. However, most cooperative control systems are asymptotically stable [4], [5], [6], [7], which means that cooperative control can achieve stability only when time approaches infinity [8]. Therefore, it has great significance to explore the cooperative control algorithm for MSVs with high control accuracy, fast convergence rate and strong anti-interference ability to improve the operation accuracy and safety. Due to the advantages of high control accuracy, fast convergence rate, the finite-time control algorithm has aroused more and more attention of researchers [9], [10]. Nevertheless, the upper bound of convergence time by the above finite-time control strategy depends on the initial state of the system, that is, the upper bound of the convergence time cannot be obtained in advance when the initial state is not available. Therefore, more and more researchers employ the fixed-time control scheme instead of the finite-time control scheme [11], [12], [13]. Moreover, it is well known that in nonlinear control, sliding mode control method has desirable robustness against uncertainties and disturbances [14], [15], [16].

The associate editor coordinating the review of this manuscript and approving it for publication was Qi Zhou.

For the above reasons, many researchers combined fixed-time control theory with sliding mode control theory and obtained excellent control effects [8], [17], [18]. In reference [8], a fixed-time non-singular terminal sliding mode was proposed and a consensus tracking control law under the directed topology was designed. In reference [17], the fixed-time sliding mode control scheme was applied to the surface vessel tracking control system, and the fixed-time neural network observer was designed to estimate the external disturbance. In some cases, the velocity information of the surface vessel cannot be accurately obtained due to the sensor noise or sensor failure. Therefore, reference [18] designed a fixed-time extended state observer to estimate the velocity and lumped disturbances, and an output feedback tracking controller was designed based on a fixed-time fast non-singular terminal sliding mode. However, there are few achievements in cooperative control for MSVs based on fixed-time sliding mode control method.

It is worth noting that the above studies only focus on the steady-state performance and ignore the transient performance (i.e., the overshoot and convergence rate). Actually, it is very challenging to guarantee a prescribed convergence performance for cooperative control system of MSVs in the uncertain marine environment. A prescribed performance control (PPC) method is proposed for the first time in [19], which can satisfy the requirements of fast convergence rate, smaller overshoot and lower steady-state error by the prescribed performance function and the error transformation. The control method was proved to be effective in many control fields [20], [21], [22]. In reference [23], a novel prescribed performance controller is proposed to guarantee the prescribed performance for the manipulator tracking error. The reference [24] designed an improved finite-time performance function for a fuzzy fault-tolerant distributed cooperative control scheme to achieve finite-time robust precision bipartite consensus tracking tasks. In reference [25], a prescribed performance function was introduced to improve the tracking performance of cooperative formation for multiagent systems. And its convergence time can be guaranteed by a user-defined function rather than the controller parameters. However, the above all prescribed performance schemes are based on backstepping control methods. There are few research achievements on fixed-time sliding mode control scheme with prescribed performance. As mentioned above, the fixed-time sliding mode control, as a high precision nonlinear controller, has great advantages in the cooperative control for MSVs. Therefore, the prescribed performance controller and the fixed-time sliding mode control can be combined in the MSVs cooperative control.

In practical engineering, most controllers update the actuator state at each sampling period, which may lead to communication resources waste and actuator wear. Due to the above disadvantages, event-triggered control has attracted more and more attention from researchers. Event-triggered control means that the state of the controller is updated when the designed event-triggered mechanism is triggered [26]. Obviously, this scheme can greatly avoid the unnecessary update of the actuator, and also reduce communication resources waste. In [27], an event-triggered strategy was applied into robust fuzzy control method to promise the high fidelity of the path following control system. In [28], the event-triggered mechanism was applied to automatic rudder control system for the surface vessel, which can significantly reduce the unnecessary actions of rudder. In addition, for the time-varying formation control problem, an event-triggered integral sliding mode control strategy was proposed in [29], which not only saved energy consumption but also avoided Zeno behavior. However, for fixed-time nonsingular terminal sliding mode control systems, there are few research achievements considering the event-triggered strategy. The reason is that it is very difficult to analyze the fixed-time nonsingular terminal sliding mode control system stability due to the error term caused by the event-triggered mechanism.

As discussed above, to begin with, although there are existing studies that apply the fixed-time nonsingular terminal sliding mode control scheme to the trajectory tracking control for single surface vessel, there are no studies that apply the fixed-time non-singular terminal sliding mode control scheme to the cooperative control for MSVs. In addition, for existing studies, most of the prescribed performance scheme is based on the backstepping control method, but few of the prescribed performance scheme based on the sliding mode control method. Furthermore, for existing studies, the event-triggered strategy has not been applied to the fixed-time nonsingular terminal sliding mode control scheme. Motivated by the aforementioned analyses and inspired by [27], [30], [31], and [40] this paper designs a fixed-time distributed cooperative event-triggered control for multiple surface vessels with prescribed performance constraint.

In summary, the main contributions are summarized as follows. First, the proposed fixed-time nonsingular terminal sliding mode control scheme is first applied to the cooperative control system for MSVs, and achieves faster convergence, higher tracking accuracy and stronger robustness. Second, the hyperbolic cosecant prescribed performance function is introduced into the cooperative control system for MSVs. In comparison with the prescribed performance function of [20] and [33], the introduced prescribed performance function has more faster convergence rate with the same initial control parameters. Third, in comparison with [13], the event-triggered strategy is introduced into fixed-time nonsingular terminal sliding mode control scheme to reduce the unnecessary updates of actuators.

This paper is organized as follows. The preliminaries and problem formation are stated in Section II. The designs of observer and controller are given in Section III and Section IV, respectively. In addition, Section V gives simulations. Section VI concludes this paper.

II. PRELIMINARIES AND PROBLEM FORMULATION

A. NOTATIONS

$\mathbb{R}^{n\times n}$ represents $n \times n$ dimensional Euclidean Space. $|\cdot|$ represents the absolute value of a scalar. $\|\cdot\|$ denotes the Euclidean norm. Denoting $x = [x_1, x_2, \ldots, x_n]^T \in \mathbb{R}^n$ and $sig^\alpha(x) = [sig^\alpha(x_1), sig^\alpha(x_2), \ldots, sig^\alpha(x_n)]^T$, where $sig^\alpha(x_i) = |x_i|^\alpha sign(x_i)$, $(i = 1, 2, \ldots, n)$, $x_i \in \mathbb{R}$, $\alpha \in (0, 1)$. $sign(\cdot)$ is expressed as:

$$sign(x) = \begin{cases} -1, & if\ x < 0 \\ 0, & if\ x = 0 \\ 1, & if\ x > 0 \end{cases} \tag{1}$$

B. GRAPH THEORY

An ordered dyadic array $\mathcal{G} = (\mathcal{V}_\mathcal{G}, \mathcal{E})$ is called a graph. $\mathcal{V}_\mathcal{G} = \{0, 1, 2, \ldots, n\}$ denotes the set of nodes. $\mathcal{E} = \{(i, j) \in \mathcal{V}_\mathcal{G} \times \mathcal{V}_\mathcal{G}\}.(i, j) \in \mathcal{E}$ indicates that the vessel j can obtain the information for the vessel i, and the vessel j is a neighbor for the vessel i. $\mathcal{N}_i = \{j \in \mathcal{V}_\mathcal{G}, (i, j) \in \mathcal{E}\}$ is a set of neighbors for the vessel i. The adjacency matrix $\mathcal{A} = [a_{ij}] \in \mathbb{R}^{n\times n}$ denotes the link relationship between vessels, where $a_{ij} = 1$, if $(i, j) \in \mathcal{E}$; otherwise $a_{ij} = 0$. If $a_{ij} = a_{ji}$, the graph is undirected; otherwise is directed. Define a Laplacian matrix $\mathcal{L} = [\ell_{ij}] \in \mathbb{R}^{n\times n}$, where $\mathcal{L} = \mathcal{D} - \mathcal{A}$, $\mathcal{D} = diag\{d_i\} \in \mathbb{R}^{n\times n}$ with $d_i = \sum_{j\in\mathcal{N}_i} a_{ij}$. In addition, A diagonal matrix $\mathcal{A}_0 = diag\{a_{i0}\}$ is used to describe a leader adjacency matrix, where $a_{i0} = 1$, if the ith vessel can get the information for the virtual leader vessel (denoted by 0); otherwise, $a_{i0} = 0$. $\mathcal{H} = \mathcal{L} + \mathcal{A}_0$ is used to describe the information exchange matrix.

Assumption 1: The communication topology among MSVs is directed, and there is at least one directed path from the virtual leader vessel to each following vessel.

Remark 1: According to [2], Assumption 1 is to ensure the connectivity of the directed communication topology, which is the necessary condition for cooperative control of MSVs.

C. DEFINITIONS AND LEMMAS

Consider the following system [9]

$$\dot{x} = f(x(t)), f(0) = 0, x(0) = 0 \tag{2}$$

where $x = [x_1, x_2, \ldots, x_n]^T$. $f(\cdot)$is regarded as a continuous nonlinear function.

Definition 1 [10]: For system (2), it is called as globally fixed-time stable, if it is globally finite-time stable and the settling time function $T(x)$ satisfying $T(x) \le T_{\max}$, where $T_{\max}$ is a positive constant.

Lemma 1 [35]: There exists a Lyapunov function $V(x)$ if it is defined on a neighborhood D for the origin and satisfies $\dot{V}(x) \le -(\alpha V(x)^p + \beta V(x)^g)^k$, then the origin of system (2) is fixed-time stable, that is, $V(x)$ can converge to $V(x) = 0$ from any initial values within the region D in the fixed-time. And the settling time satisfies $T \le \frac{1}{\alpha^k(1-pk)} + \frac{1}{\beta^k(gk-1)}$, where α, β, p, g, k are positive constants, and $pk < 1, gk > 1$.

Lemma 2 [31]: There exists a Lyapunov function $V(x)$, if it satisfies $\dot{V}(x) \le -(\alpha V(x)^p + \beta V(x)^g)^k + \Upsilon$, where α, β, p, g, k are positive constants, $pk < 1, gk > 1$ and $0 < \Upsilon < \infty$, then the system is practical fixed-time stable. And the residual set is given by $\left\{\lim_{t\to T} x \middle| V(x) \le \min\left\{\alpha^{-\frac{1}{p}}(\frac{\Upsilon}{1-\theta^k})^{\frac{1}{kp}}, \beta^{-\frac{1}{g}}(\frac{\Upsilon}{1-\theta^k})^{\frac{1}{kg}}\right\}\right\}$, where θ is a constant and satisfies $0 < \theta \le 1$. Moreover, the settling time satisfies $T \le \frac{1}{\alpha^k\theta^k(1-pk)} + \frac{1}{\beta^k\theta^k(gk-1)}$.

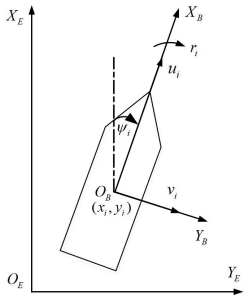

FIGURE 1. Earth-fixed frame and body-fixed frame.

D. SYSTEM MODELING AND PROBLEM FORMULATION

There exists a networked of n MSVs, labeled as 1 to n. Let $\eta_i = [x_i, y_i, \psi_i]^T \in \mathbb{R}^3$ denotes the position and yaw angle vector for the ith vessel in earth-fixed frame $X_E O_E Y_E$ as shown in Figure 1. Let $\upsilon_i = [u_i, v_i, r_i]^T \in \mathbb{R}^3$ denotes the velocity vector of the i-th surface vessel expressed in the body-fixed frame $X_B O_B Y_B$. Then, the mathematic model of the ith vessel is expressed by [30].

$$\dot{\eta}_i = R_i(\psi_i)\upsilon_i \tag{3}$$

$$M_i\dot{\upsilon}_i = -D_i(\upsilon_i)\upsilon_i - C_i(\upsilon_i)\upsilon_i + \tau_i + \tau_{id} \tag{4}$$

where $\tau_{id} = [\tau_{idu}, \tau_{idv}, \tau_{idr}]^T \in \mathbb{R}^3$ consists of the total environmental disturbances caused by wind, waves, ocean currents in surge, sway and yaw, respectively. $\tau_i = [\tau_{iu}, \tau_{iv}, \tau_{ir}]^T \in \mathbb{R}^3$ is the control input produced by thrusters. $M_i \in \mathbb{R}^{3\times3}$ denotes the inertia matrix, $D_i(\upsilon_i) \in \mathbb{R}^{3\times3}$ denotes the damping matrix. $C_i(\upsilon_i) \in \mathbb{R}^{3\times3}$ denotes the Coriolis centripetal force matrix caused by hydrodynamic forces. The M_i, $C_i(\upsilon_i)$ and $D_i(\upsilon_i)$ are given as:

$$M_i = \begin{bmatrix} m_{11} & 0 & 0 \\ 0 & m_{22} & m_{23} \\ 0 & m_{32} & m_{33} \end{bmatrix} \tag{5}$$

$$C_i(\upsilon_i) = \begin{bmatrix} 0 & 0 & -m_{22}\upsilon - m_{23}r \\ 0 & 0 & m_{11}u \\ m_{22}\upsilon + m_{23}r & -m_{11}u & 0 \end{bmatrix} \tag{6}$$

$$D_i(\upsilon_i) = \begin{bmatrix} d_{11} & 0 & 0 \\ 0 & d_{22} & d_{23} \\ 0 & d_{32} & d_{33} \end{bmatrix} \tag{7}$$

For detailed definitions of the inertia matrix, the coriolis centripetal force matrix and the damping matrix, please refer to [36]. $R_i(\psi_i) \in \mathbb{R}^{3\times3}$ denotes the

rotation matrix and given by:

$$R_i(\psi_i) = \begin{bmatrix} \cos\psi_i & -\sin\psi_i & 0 \\ \sin\psi_i & \cos\psi_i & 0 \\ 0 & 0 & 1 \end{bmatrix} \tag{8}$$

with the following properties [9]:

$$\dot{R}_i(\psi_i) = R_i(\psi_i) S_i(r_i) \tag{9}$$

$$R_i^T(\psi_i) S_i(r_i) R_i(\psi_i) = R_i(\psi_i) S_i(r_i) R_i^T(\psi_i) = S_i(r_i) \tag{10}$$

$$S_i(r_i) = \begin{bmatrix} 0 & -r_i & 0 \\ r_i & 0 & 0 \\ 0 & 0 & 0 \end{bmatrix} \tag{11}$$

$$R_i^T(\psi_i) R_i(\psi_i) = I_3 \tag{12}$$

$$\|R_i(\psi_i)\| = 1 \tag{13}$$

For the convenience of writing, we have $R_i = R_i(\psi_i)$ and $S_i = S_i(r_i)$.

Assumption 2: The reference signal η_d is smooth enough, and its first and second derivatives exist and are bounded.

Remark 2: From [37], to make the vessel move smoothly, it is usually necessary to make the reference signal smooth enough that the first and second derivatives exist and are bounded. Thus, the Assumption 2 is reasonable.

Assumption 3: The time-varying environmental disturbance τ_{id} and its time derivation $\dot{\tau}_{id}$ are bounded, that is, there exist unknown positive constants $\bar{\tau}_{id}$ and ϖ_i, such that $\|\tau_{id}\| \le \bar{\tau}_{id}$ and $\|\dot{\tau}_{id}\| \le \varpi_i$.

Remark 3: From [2], the time-varying environmental disturbances are generally considered as slowly-varying disturbances with limited energy. Thus, the time-varying environmental disturbances acting on the surface vessel can be regarded as finite change rates and bounded signals. Thus, the Assumption 3 is reasonable.

Assumption 4: The parameter matrix M_i for the ith vessel is known.

Remark 4: From [13], the parameter matrix M_i for the ith vessel is easy to measure. Thus, the Assumption 4 is reasonable.

The control objective for this paper is to design a fixed time distributed cooperative event-triggered control scheme for each MSV with unknown environmental disturbances, model parameter uncertainties, unavailable velocities and output constraints such that the reference signal η_d can be tracked within fixed time.

III. DESIGN OF FxESO

For simplicity, a new auxiliary velocity vector is introduced as follows:

$$w_i = R_i \upsilon_i \tag{14}$$

where $w_i = [w_{iu}, w_{iv}, w_{ir}]^T \in \mathbb{R}^3$.

Applying (9)–(13), the model (3)-(4) for ith surface vessel are rewritten as

$$\dot{\eta}_i = w_i \tag{15}$$

$$\dot{w}_i = R_i M_i^{-1} \tau_i + \Gamma_i \tag{16}$$

$$\dot{\eta}_d = w_d \tag{17}$$

where $\Gamma_i = R_i S_i \upsilon_i - R_i M_i^{-1} C_i(\upsilon_i)\upsilon_i - R_i M_i^{-1} D_i(\upsilon_i)\upsilon_i + R_i M_i^{-1}\tau_{id}$, $\eta_d = [x_d, y_d, \psi_d]^T$ is the desired position vector and $w_d = [w_{du}, w_{dv}, w_{dr}]^T$ is the desired auxiliary velocity vector.

Remark 5: From [10], Γ_i is continuously differentiable and bounded and it includes model parameter uncertainties and time-varying environmental disturbances. Thus, there exist a constant Γ_{id}, $\|\dot{\Gamma}(t)\| \le H_n < \Gamma_{id}$ with $0 < \Gamma_{id} < \infty$.

In this part, the FxESO is designed to estimate velocity and lumped disturbances for the each vessel. $\hat{\eta}_i$ is an estimate of η_i. Then, the FxESO is designed as [38]

$$\begin{cases} \dot{\hat{\eta}}_i = \hat{w}_i + \mu_1 sig^{\alpha_1}(\tilde{\eta}_i) + \varepsilon_1 sig^{\beta_1}(\tilde{\eta}_i) \\ \dot{\hat{w}}_i = \hat{\Gamma}_i + \mu_2 sig^{\alpha_2}(\tilde{\eta}_i) + \varepsilon_2 sig^{\beta_2}(\tilde{\eta}_i) + R_i M_i^{-1}\tau_i \\ \dot{\hat{\Gamma}}_i = \mu_3 sig^{\alpha_3}(\tilde{\eta}_i) + \varepsilon_3 sig^{\beta_3}(\tilde{\eta}_i) + \Gamma_{id} sign(\tilde{\eta}_i), \end{cases} \tag{18}$$

where $\tilde{\eta}_i = \eta_i - \hat{\eta}_i$, $\alpha_m \in (0,1)$, $\beta_m \in (1,\infty)$, $(m = 1,2,3)$. $\alpha_m = m\bar{\alpha} - (m-1)$, $\beta_m = m\bar{\beta} - (m-1)$, $\bar{\alpha} \in (1-l_1, 1)$, $\bar{\beta} \in (1, 1+l_2)$ with small enough constants $l_1 > 0$, $l_2 > 0$. The observer gains are designed to guarantee the following matrix are Hurwitz.

$$P_1 = \begin{bmatrix} -\mu_1 & 1 & 0 \\ -\mu_2 & 0 & 1 \\ -\mu_3 & 0 & 0 \end{bmatrix}, \quad P_2 = \begin{bmatrix} -\varepsilon_1 & 1 & 0 \\ -\varepsilon_2 & 0 & 1 \\ -\varepsilon_3 & 0 & 0 \end{bmatrix}$$

Then, w_i and Γ_i can be observed by $\hat{w}_i$ and $\hat{\Gamma}_i$ respectively.

Theorem 1: Based on the Assumption 3 and Remark 3, the velocity w_i and the lumped disturbance Γ_i can be estimated by the FxESO (18), and the estimation errors can converge within fixed time. The convergence time is bounded by

$$T_1 \le \frac{\lambda_{\max}^{1-\bar{\alpha}}(\Omega_1)}{\gamma_1(1-\bar{\alpha})} + \frac{1}{\gamma_2(\bar{\beta}-1)\hbar^{\bar{\beta}-1}} \tag{19}$$

where $\gamma_1 = \lambda_{\min}(Q_1)/\lambda_{\max}(\Omega_1)$, $\gamma_2 = \lambda_{\min}(Q_2)/\lambda_{\max}(\Omega_2)$, the positive constant $\hbar \le \lambda_{\min}(\Omega_2)$. Q_1, Q_2, Ω_1 and Ω_2 are nonsingular, symmetric and positive definite matrices. Moreover, the above parameter matrices are satisfied with $P_1^T\Omega_1 + \Omega_1 P_1 = -Q_1$ and $P_2^T\Omega_2 + \Omega_2 P_2 = -Q_2$, respectively.

Proof: The estimation errors are as follows

$$\begin{cases} \tilde{e}_{i1} = \eta_i - \hat{\eta}_i \\ \tilde{e}_{i2} = w_i - \hat{w}_i \\ \tilde{e}_{i3} = \Gamma_i - \hat{\Gamma}_i \end{cases} \tag{20}$$

Taking the derivative of (20), yields

$$\begin{cases} \dot{\tilde{e}}_{i1} = \tilde{e}_{i2} - \mu_1 sig^{\alpha_1}(\tilde{e}_{i1}) - \varepsilon_1 sig^{\beta_1}(\tilde{e}_{i1}) \\ \dot{\tilde{e}}_{i2} = \tilde{e}_{i3} - \mu_2 sig^{\alpha_2}(\tilde{e}_{i1}) - \varepsilon_2 sig^{\beta_2}(\tilde{e}_{i1}) \\ \dot{\tilde{e}}_{i3} = \dot{\Gamma}_i - \mu_3 sig^{\alpha_3}(\tilde{e}_{i1}) - \varepsilon_3 sig^{\beta_3}(\tilde{e}_{i1}) - \Gamma_{id} sign(\tilde{e}_{i1}) \end{cases} \tag{21}$$

From [35], in order to prove that the estimation errors can converge to zero within fixed time, The process is divided into the following steps:

1). Prove that the following error system converges to zero within a fixed time.

$$\begin{cases} \dot{\tilde{e}}_{i1} = \tilde{e}_{i2} - \mu_1 sig^{\alpha_1}(\tilde{e}_{i1}) - \varepsilon_1 sig^{\beta_1}(\tilde{e}_{i1}) \\ \dot{\tilde{e}}_{i2} = \tilde{e}_{i3} - \mu_2 sig^{\alpha_2}(\tilde{e}_{i1}) - \varepsilon_2 sig^{\beta_2}(\tilde{e}_{i1}) \\ \dot{\tilde{e}}_{i3} = -\mu_3 sig^{\alpha_3}(\tilde{e}_{i1}) - \varepsilon_3 sig^{\beta_3}(\tilde{e}_{i1}) \end{cases} \tag{22}$$

The proof does not much differ from that of Theorem 2 in [10] and thus is omitted here for space. Then, $\tilde{e}_{im}(m = 1, 2, 3)$ can converge to zero in fixed time.

2). Referring to [35], the following equation can be proved

$$\dot{\tilde{e}}_{i3} = \dot{\Gamma}_i - \Gamma_{id} sign(\tilde{e}_{i1}) = 0, \quad t \geq T_1 \tag{23}$$

IV. CONTROLLER DESIGN

In this section, a fixed-time distributed cooperative event-triggered sliding mode controller with prescribed performance constraints combined with the FxESO is designed. The controller design process is divided into the following steps.

Step 1: Define the tracking errors for ith vessel based on the communication relationship as follows:

$$z_{i1} = \sum_{j \in \mathcal{N}_i} a_{ij} \left(\eta_i - \eta_j - \vartheta_{ij}\right) + a_{i0} \left(\eta_i - \eta_d - \vartheta_i\right) \tag{24}$$

$$\hat{z}_{i2} = a_{id}\hat{w}_i - \sum_{j \in \mathcal{N}_i} a_{ij}\hat{w}_j - a_{i0}w_d \tag{25}$$

where $\mathcal{N}_i$, a_{ij} and a_{i0} are defined in the Section II, ϑ_i denotes the constant expected relative position vector from the virtual leader vessel to the ith vessel, ϑ_{ij} denotes the constant expected relative position vector from the ith vessel to the neighboring jth vessel and $a_{id} = a_{i0} + d_i$. $\hat{z}_{i2}$ is an estimate of z_{i2}.

Remark 6: Based on the FxESO in (18) and Theorem 1, $\hat{z}_{i2} = z_{i2}$ for $t \geq T_1$, thus, (25) will be transferred as

$$\hat{z}_{i2} = z_{i2} = \dot{z}_{i1} = a_{id}w_i - \sum_{j \in \mathcal{N}_i} a_{ij}w_j - a_{i0}w_d \tag{26}$$

The derivative of (26) is given by

$$\dot{\hat{z}}_{i2} = \dot{z}_{i2} = a_{id}R_i M_i^{-1}\tau_i + a_{id}\Gamma_i - \sum_{j \in N_i} a_{ij}\dot{w}_j - a_{i0}\dot{w}_d \tag{27}$$

Step 2: Design prescribed performance constraints and error transformation:

The prescribed performance constraints can be designed as:

$$-\chi_{im}(t) < z_{i1m}(t) < \chi_{im}(t), \quad \forall t > 0, \ (m = u, v, r) \tag{28}$$

where $\chi_{im}(t)$ is a smooth prescribed performance function (PPF) and it can be described as [41]

$$\chi_{im}(t) = \mathrm{csch}(a_p t + \chi_{im0}) + \chi_{im\infty}, \quad (m = u, v, r) \tag{29}$$

where $\mathrm{csch}(x) = 2/(e^x - e^{-x})$, a_p is a prescribed positive constant which can adjust the convergence time, and $\chi_{im\infty}$ represents the terminal value of $\chi_{im}(t)$ that determines the steady-state error. χ_{im0} is a control parameter that determines the initial value of $\chi_{im}(0)$ and it is worth noting that $\chi_{im}(0) \neq \chi_{im0}$.

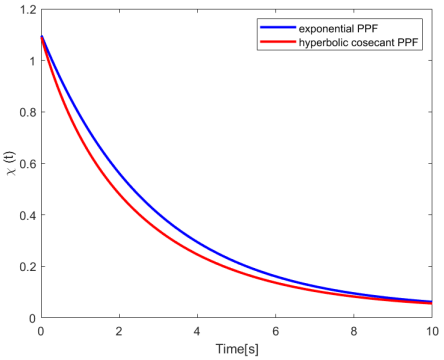

FIGURE 2. Simulation comparison for the exponential PPF and the hyperbolic cosecant PPF.

Assumption 5: The initial tracking errors of all vessels are chosen such that $-\chi_{im}(0) < z_{i1m}(0) < \chi_{im}(0)$, $(m = u, v, r)$.

Remark 7: Compared with the existing exponential prescribed performance function (exponential PPF) $\chi_{im}(t) = (a_{p0} - \chi_{im\infty})e^{-a_p t} + \chi_{im\infty}$, the introduced hyperbolic cosecant prescribed performance function (hyperbolic cosecant PPF) has more faster convergence rate with the same initial control parameters. The simulation comparison is shown in Figure 2, where parameters are set to be $a_p = 0.5$, $a_{p0} = 1.1$, $\chi_{im0} = 0.8375$, $\chi_{im\infty} = 0.05$.

In order to satisfy the prescribed performance, the following transformation is carried out:

$$z_{i1m}(t) = \chi_{im}(t)\Phi_{im}(Z_{i1m}(t)), \quad \forall t \geq 0, \ (m = u, v, r) \tag{30}$$

where $\Phi_{im}(Z_{i1m}(t)) = \frac{e^{Z_{i1m}(t)} - e^{-Z_{i1m}(t)}}{e^{Z_{i1m}(t)} + e^{-Z_{i1m}(t)}}$, $Z_{i1m}(t)$ is the transformation error, since the function $\Phi_{im}(Z_{i1m}(t))$ is strictly monotonic increasing and $\frac{\partial \Phi_{im}}{\partial Z_{i1m}(t)} = \frac{4}{(e^{Z_{i1m}(t)} + e^{-Z_{i1m}(t)})^2} > 0$, then we can get the transformation errors as follows

$$\begin{aligned} Z_{i1m}(t) &= \Phi_{im}^{-1}\left(\frac{z_{i1m}}{\chi_{im}}\right) \\ &= \frac{1}{2}\ln\frac{1 + z_{i1m}(t)/\chi_{im}(t)}{1 - z_{i1m}(t)/\chi_{im}(t)}, \quad (m = u, v, r) \end{aligned} \tag{31}$$

Remark 8: By solving (31), we can find that (31) is equivalent to (28) if $Z_{i1m}(t)$ is bounded. Therefore, the constrained prescribed performance control problem can be translated into the unconstrained control problem.

The derivative of (31) is given by

$$Z_{i2m} = \dot{Z}_{i1m} = g_{im}(z_{i2m} - z_{i1m}\dot{\chi}_{im}/\chi_{im}), \quad (m = u, v, r) \tag{32}$$

where $g_{im} = \frac{1}{\chi_{im}(1 - z_{i1m}/\chi_{im})(1 + z_{i1m}/\chi_{im})}$.

Taking the derivative of (32), it yields to

$$\begin{aligned} \dot{Z}_{i2m} = {} & \dot{g}_{im}\left(z_{i2m} - \frac{z_{i1m}\dot{\chi}_{im}}{\chi_{im}}\right) \\ & - g_{im}\frac{z_{i2m}\dot{\chi}_{im}\chi_{im} + z_{i1m}\ddot{\chi}_{im}\chi_{im} - z_{i1m}\dot{\chi}_{im}^2}{\chi_{im}^2} \\ & + g_{im}\dot{z}_{i2m}, \quad (m = u, v, r) \end{aligned} \tag{33}$$

For ease of description, equations (32) and (33) will be changed as the vector form

$$Z_{i2} = \dot{Z}_{i1} = diag(G_i)(z_{i2} - diag(\dot{\chi}_i)[diag(\chi_i)]^{-1} z_{i1}) \quad (34)$$

$$\dot{Z}_{i2} = diag(\dot{G}_i)(z_{i2} - diag(\dot{\chi}_i)[diag(\chi_i)]^{-1} z_{i1}) - diag(G_i)A_i + diag(G_i)\dot{z}_{i2} \quad (35)$$

where $A_i = [A_{iu} A_{iv} A_{ir}]^T$, $A_{im} = (z_{i2m}\dot{\chi}_{im}\chi_{im} + z_{i1m}\ddot{\chi}_{im}\chi_{im} - z_{i1m}\dot{\chi}_{im}^2)/\chi_{im}^2$, $(m = u, v, r)$, $G_i = [g_{iu}\ g_{iv}\ g_{ir}]^T$, $\dot{G}_i = [\dot{g}_{iu}\ \dot{g}_{iv}\ \dot{g}_{ir}]^T$ and $\chi_i = [\chi_{iu}\ \chi_{iv}\ \chi_{ir}]^T$.

Substituting (27) into (35), yields

$$\dot{Z}_{i2} = B_i + a_{id} diag(G_i) R_i M_i^{-1} \tau_i + a_{id} diag(G_i)\Gamma_i - diag(G_i)\sum_{j\in N_i} a_{ij}\dot{w}_j - a_{i0} diag(G_i)\dot{w}_d \quad (36)$$

where $B_i = diag(\dot{G}_i)(z_{i2} - diag(\dot{\chi}_i)[diag(\chi_i)]^{-1} z_{i1}) - diag(G_i)A_i$.

Step 3: Design FxNTSMM

In this section, the FxNTSMM [31] for ith vessel is designed as follows

$$S_i = \beta(Z_{i1})Z_{i1} + sig^{r_2}(Z_{i2}) \quad (37)$$

where $\beta(Z_{i1}) = diag([\beta_1(Z_{i11}), \beta_2(Z_{i12}), \beta_3(Z_{i13})])$, $\beta_m(Z_{i1m})$, $(m = u, v, r)$ as follows

$$\beta_m(Z_{i1m}) = \begin{cases} (a_s|Z_{i1m}|^{r_1-\frac{1}{r_2}} + b_s)^{r_2}, & |Z_{i1m}| \geq \Theta \\ (a_{s1}|Z_{i1m}|^{r_1-\frac{1}{r_2}} + a_{s2}|Z_{i1m}|^{2-\frac{1}{r_2}} + b_s), & |Z_{i1m}| < \Theta \end{cases} \quad (38)$$

where $a_s > 0$, $b_s > 0$, $a_{s1} = a_s(2 - r_1)\Theta^{(r_1-1)}$, $r_1 > 1$, $1 < r_2 < 2$ and $0 < \Theta \leq 1$.

Theorem 2: With the FxESO (18), if the sliding mode surface $S_i = 0$, then Z_{i1} and Z_{i2} converge to zero within the fixed convergence time T_2.

Proof: If $S_i = 0$ is satisfied, the designed sliding mode surface (37) will be rewritten as follows

$$\dot{Z}_{i1m} = \begin{cases} -a_s sig^{r_1}(Z_{i1m}) - b_s sig^{\frac{1}{r_2}}(Z_{i1m}), & |Z_{i1m}| \geq \Theta \\ -a_{s1}Z_{i1m} - a_{s2}sign(Z_{i1m})z_{i1m}^2 - b_s sig^{\frac{1}{r_2}}(Z_{i1m}), & |Z_{i1m}| < \Theta \end{cases} \quad (39)$$

In order to facilitate the proof, define a new variable $\zeta_m = |Z_{i1m}|^{1-\frac{1}{r_2}}$. Combining with (38), the derivative for ζ_{im}, yields

$$\dot{\zeta}_{im} = \begin{cases} -(1 - \frac{1}{r_2})(a_s\zeta_{im}^{1+r_{\zeta 1}} + b_s), & |\zeta_{im}| \geq \Lambda \\ -(1 - \frac{1}{r_2})(a_{s1}\zeta_{im} + a_{s2}\zeta_{im}^{1+r_{\zeta 2}} + b_s), & |\zeta_{im}| < \Lambda \end{cases} \quad (40)$$

where $r_{\zeta 1} = \frac{r_2(r_1-1)}{r_2-1}$, $r_{\zeta 2} = \frac{r_2}{r_2-1}$ and $\Lambda = \Theta^{(1-1/r_2)}$.

By integrating and solving (40), the convergence time for Z_{i1} and Z_{i2} are determined as

$$\begin{aligned} T_2 &= T_1 + \int_{\Lambda}^{+\infty} \frac{r_2}{r_2-1}\frac{1}{a_s\zeta_{im}^{1+r_{\zeta 1}} + b_s} d\zeta_{im} \\ &\quad + \int_{0}^{\Lambda} \frac{r_2}{r_2-1}\frac{1}{a_{s1}\zeta_{im} + a_{s2}\zeta_{im}^{1+r_{\zeta 2}} + b_s} d\zeta_{im} \\ &\leq T_1 + \frac{r_2}{r_2-1}\int_{\Lambda}^{+\infty} \frac{1}{a_s\zeta_{im}^{1+r_{\zeta 1}}} d\zeta_{im} \\ &\quad + \frac{r_2}{r_2-1}\int_{0}^{\Lambda} \frac{1}{a_{s1}\zeta_{im} + b_s} d\zeta_{im} \\ &\leq T_1 + \frac{\Lambda^{-r_{\zeta 1}}}{a_s(r_1-1)} + \frac{r_2}{r_2-1}\frac{1}{a_{s1}}\ln(\frac{a_{s1}\Lambda}{b_s} + 1) \end{aligned} \quad (41)$$

This completes the Theorem 2.

Remark 9: We know from (37) that the designed sliding mode manifold can be divided into two fixed-time terminal sliding mode manifolds: $S_1 = \dot{x} + a_s sig^{r_1}(x) + b_s sig^{1/r_2}(x)$, $|x_m| \geq \Theta$ and $S_2 = \dot{x} + a_{s1}x + a_{s2}sign(x)x^2 + b_s sig^{1/r_2}(x)$, $|x_m| < \Theta$. When $|x_m| < \Theta$, the system states can be smoothly switched from sliding mode manifold S_1 to sliding mode manifold S_2. According to S_2, the nonlinear term $sig^{1/r_2}(x)$, $(r_2 > 1)$ is regarded as the dominating term rather than a quadratic function $a_{s1}x + a_{s2}sign(x)x^2$ replaced $sig^{1/r_2}(x)$, $(r_2 > 1)$ in [39] to avoid the singularity problem. Moreover, the nonlinear term $sig^{r_1}(x)$, $(r_1 > 1)$ is replaced by the quadratic function $a_{s1}x + a_{s2}sign(x)x^2$, which dominates over $sig^{r_1}(x)$, $(r_1 > 1)$ nearby the origin. Therefore, compared with fixed-time terminal sliding mode manifold, the designed sliding mode manifold has the advantages of non-singularity and faster convergence.

Step 3: Design the fixed-time nonsingular terminal sliding mode event-triggered control law with prescribed performance constraint.

Combining with the FxESO in (18) and FxNTSMM in (37), the control law for this paper is designed as

$$\begin{aligned} \omega_{\tau i}(t) = -\bar{M}_i[&\frac{1}{r_2}(\tilde{\beta}(Z_{i1}) + \beta(Z_{i1}))sig^{2-r_2}(Z_{i2}) \\ &+ \frac{1}{r_2}diag\{\rho(|Z_{i2}|^{r_2-1})\}diag\{|Z_{i2}|^{1-r_2}\} \\ &\cdot(\alpha sig^{r_3}(S_i) + \beta sig^{r_4}(S_i)) + B_i \\ &+ a_{id}diag(G_i)\hat{\Gamma}_i - diag(G_i)\sum_{j\in N_i} a_{ij}\dot{w}_j \\ &- a_{i0}diag(G_i)\dot{w}_d] \end{aligned} \quad (42)$$

where $\bar{M}_i = M_i R_i^{-1}[diag(G_i)]^{-1}/a_{id}$, α, β, r_3 and r_4 are positive constants, $r_3 \in (0, 1)$ and $r_4 \in (1, +\infty)$.

$$\rho(|Z_{i2m}|^{r_2-1}) = \begin{cases} \sin(\frac{\pi}{2}\frac{|Z_{i2m}|^{r_2-1}}{\iota}), & |Z_{i2m}|^{r_2-1} < \iota \\ 1, & |Z_{i2m}|^{r_2-1} \geq \iota \end{cases} \quad (43)$$

where $\iota > 0$ is a design parameter. $\rho(|Z_{i2m}|^{r_2-1})$ is nonnegative function and satisfies $\rho(|Z_{i2m}|^{r_2-1})/|Z_{i2m}|^{r_2-1} \to (\pi/2\iota)$ when $|Z_{i2m}|^{r_2-1} \to 0$.

$$\tilde{\beta}_m(Z_{i1m}) = \begin{cases} r_2 a_s (r_1 - \frac{1}{r_2})(a_s|Z_{i1m}|^{r_1-\frac{1}{r_2}} + b_s)^{r_2-1}|Z_{i1m}|^{r_1-\frac{1}{r_2}}, \\ \qquad\qquad |Z_{i1m}| \geq \Theta \\ r_2(a_{s1}|Z_{i1m}|^{1-\frac{1}{r_2}} + a_{s2}|Z_{i1m}|^{2-\frac{1}{r_2}} + b_s)^{r_2-1} \\ \{a_{s1}(1-\frac{1}{r_2})|Z_{i1m}|^{1-\frac{1}{r_2}} + a_{s2}(2-\frac{1}{r_2})|Z_{i1m}|^{2-\frac{1}{r_2}}\}, \\ \qquad\qquad |Z_{i1m}| < \Theta \end{cases} \tag{44}$$

The triggering condition is selected as

$$\tau_{im}(t) = \omega_{\tau im}(t_{km}), \quad \forall t \in [t_{km}, t_{(k+1)m}), \ (m = u, v, r) \tag{45}$$

with

$$t_{(k+1)m} = \inf\{t > t_{km} : |e_{im}(t)| \geq \sigma_m\}, \quad t_{1m} = 0 \tag{46}$$

where $e_{im}(t) = \omega_{\tau im}(t) - \tau_{im}(t)$, σ_m is a positive constant.

Theorem 3: For the MSVs dynamic model in (3) and (4), we can design the controller as (45), and the FxESO in (18), the tracking errors with constraints Z_{i1} and Z_{i2} finally converge into the small regions within fixed time and the upper bound of the convergence time is $T \leq T_2 + T_3$.

Proof: Define a Lyapunov function candidate as

$$V = \frac{1}{2} S_i^T S_i \tag{47}$$

Taking the derivative of (47), yields

$$\begin{aligned} \dot{V} &= S_i^T \dot{S}_i \\ &= S_i^T [\frac{d\beta(Z_{i1})}{dt} Z_{i1} + \beta(Z_{i1}) Z_{i2} \\ &\quad + r_2 diag\{|Z_{i2}|^{r_2-1}\} \dot{Z}_{i2}] \end{aligned} \tag{48}$$

Substituting (36) into (48), yields

$$\begin{aligned} \dot{V} = S_i^T [&\frac{d\beta(Z_{i1})}{dt} Z_{i1} + \beta(Z_{i1}) Z_{i2} + r_2 diag\{|Z_{i2}|^{r_2-1}\} \\ &\cdot \{B_i + a_{id} diag(G_i) R_i M_i^{-1} \tau_i + a_{id} diag(G_i) \Gamma_i \\ &- diag(G_i) \sum_{j \in N_i} a_{ij} \dot{w}_j - a_{i0} diag(G_i) \dot{w}_d\}] \end{aligned} \tag{49}$$

According to (45) and (46), one has $|\omega_{\tau im}(t_{km}) - \tau_{im}(t)| \leq \sigma_m$. There exist time-varying functions $\mu_m (m = u, v, r)$ satisfying $|\mu_m| \leq 1$. Then, $\omega_{\tau im} = \tau_{im} + \mu_m \sigma_m (m = u, v, r)$. (49) is converted to

$$\begin{aligned} \dot{V} = S_i^T [&\frac{d\beta(Z_{i1})}{dt} Z_{i1} + \beta(Z_{i1}) Z_{i2} + r_2 diag\{|Z_{i2}|^{r_2-1}\} \\ &\cdot \{B_i + a_{id} diag(G_i) R_i M_i^{-1} (\omega_{\tau i} - \mu\sigma) + a_{id} diag(G_i) \\ &\cdot \Gamma_i - diag(G_i) \sum_{j \in N_i} a_{ij} \dot{w}_j - a_{i0} diag(G_i) \dot{w}_d\}] \end{aligned} \tag{50}$$

where $\mu = diag([\mu_u, \mu_v, \mu_r])$, $\sigma = [\sigma_u, \sigma_v, \sigma_r]^T$, $\sigma_m (m = u, v, r)$ is defined in (46). By applying the Theorem 1 and (42), yields

$$\begin{aligned} \dot{V} = S_i^T [&\frac{d\beta(Z_{i1})}{dt} Z_{i1} + \beta(Z_{i1}) Z_{i2} - r_2 diag\{|Z_{i2}|^{r_2-1}\} \\ &\cdot \{\frac{1}{r_2}(\tilde{\beta}(Z_{i1}) + \beta(Z_{i1})) \cdot sig^{2-r_2}(Z_{i2}) \\ &+ \frac{1}{r_2} diag\{\rho(|Z_{i2}|^{r_2-1}) diag\{|Z_{i2}|^{1-r_2}\} \\ &\cdot (\alpha sig^{r_3}(S_i) + \beta sig^{r_4}(S_i)) \\ &+ a_{id} diag(G_i) R_i M_i^{-1} \mu\sigma\}] \end{aligned} \tag{51}$$

Subsequently, we have

$$\begin{aligned} \dot{V} = S_i^T [&\frac{d\beta(Z_{i1})}{dt} Z_{i1} + \beta(Z_{i1}) Z_{i2} - diag\{|Z_{i2}|^{r_2-1}\} \\ &\cdot \{(\tilde{\beta}(Z_{i1}) + \beta(Z_{i1})) sig^{2-r_2}(Z_{i2})\} \\ &- diag\{\rho(|Z_{i2}|^{r_2-1})\}(\alpha sig^{r_3}(S_i) + \beta sig^{r_4}(S_i)) \\ &- a_{id} r_2 diag\{|Z_{i2}|^{r_2-1}\} diag(G_i) R_i M_i^{-1} \mu\sigma] \end{aligned} \tag{52}$$

According to $\frac{d\beta(Z_{i1})}{dt} Z_{i1} = \tilde{\beta}(Z_{i1}) Z_{i2}$, (52) can be rewritten as follows

$$\begin{aligned} \dot{V} = S_i^T [&-diag\{\rho(|Z_{i2}|^{r_2-1})\}(\alpha sig^{r_3}(S_i) + \beta sig^{r_4}(S_i)) \\ &- a_{id} r_2 diag\{|Z_{i2}|^{r_2-1}\} diag(G_i) R_i M_i^{-1} \mu\sigma] \end{aligned} \tag{53}$$

According to $-S_i^T a_{id} r_2 diag\{|Z_{i2}|^{r_2-1}\} diag(G_i) R_i M_i^{-1} \mu\sigma \leq \left| S_i^T a_{id} r_2 diag\{|Z_{i2}|^{r_2-1}\} diag(G_i) R_i M_i^{-1} \mu\sigma \right| = \Upsilon_i$, where $0 < \Upsilon_i < \infty$, yeilds

$$\begin{aligned} \dot{V} &\leq S_i^T [-diag\{\rho(|Z_{i2}|^{r_2-1})\}(\alpha sig^{r_3}(S_i) + \beta sig^{r_4}(S_i))] \\ &\quad + \Upsilon_i \\ &\leq -\alpha \sum_{m=u,v,r} \rho(|Z_{i2m}|^{r_2-1}) |S_{im}|^{1+r_3} \\ &\quad - \beta \sum_{m=u,v,r} \rho(|Z_{i2m}|^{r_2-1}) |S_{im}|^{1+r_4} + \Upsilon_i \end{aligned} \tag{54}$$

According to Lemma 2, we have

$$\dot{V} \leq -c_1 V^{\frac{1+r_3}{2}} - c_2 V^{\frac{1+r_4}{2}} + \Upsilon_i \tag{55}$$

where $c_1 = \min\left\{\alpha\rho(|Z_{i2m}|^{r_2-1}) 2^{\frac{1+r_3}{2}}\right\}$ and $c_2 = \min\left\{\beta\rho(|Z_{i2m}|^{r_2-1}) 2^{\frac{1+r_4}{2}} 3^{\frac{1-r_4}{2}}\right\}$.

According to (43), the system state will be divided into two regions:

$$\Pi_1 = \left\{(Z_{i1m}, Z_{i2m}) \middle| |Z_{i2m}|^{r_2-1} \geq \iota\right\} \tag{56}$$

$$\Pi_2 = \left\{(Z_{i1m}, Z_{i2m}) \middle| |Z_{i2m}|^{r_2-1} < \iota\right\} \tag{57}$$

Case 1: If $|Z_{i2m}|^{r_2-1} \geq \iota$, according to (43), we have $\rho(|Z_{i2m}|^{r_2-1}) = 1$. From Lemma 2, the system is the practical fixed-time stability. And, the system states can converge to the following region:

$$W_i = \left\{ \lim_{t \to T_3} S_i \middle| V_i \leq \min \left\{ \begin{matrix} c_1^{-\frac{2}{1+r_3}} (\frac{\Upsilon_i}{1-\theta})^{\frac{2}{1+r_3}}, \\ c_2^{-\frac{2}{1+r_4}} (\frac{\Upsilon_i}{1-\theta})^{\frac{2}{1+r_4}} \end{matrix} \right\} \right\} \tag{58}$$

The upper bound for the convergence time T_3 is as follows

$$T_3 \leq \frac{1}{c_1\theta(1-\frac{1+r_3}{2})} + \frac{1}{c_2\theta(\frac{1+r_4}{2}-1)} \tag{59}$$

where θ is a constant and satisfies $0 < \theta \leq 1$.

Case 2: For $|Z_{i2m}|^{r_2-1} < \iota$, we will prove that the region Π_2 is not an attractor except the origin. If $Z_{i2} \to 0$, substituting (45) into (36), yield

$$\dot{Z}_{i2} = -\frac{\pi}{2\iota r_2}(\alpha sig^{r_3}(S_i) + \beta sig^{r_4}(S_i)) - a_{id} diag(G_i) R_i M_i^{-1} \mu\sigma \tag{60}$$

Therefore, if the sufficient small parameter ι is selected, there is $\dot{Z}_{i2}S_i < 0$, which implies that Π_2 is not an attractor and the system states will escape the region Π_2 in a very short time [31]. It is obvious that the system states Z_{i1} and Z_{i2} are decreasing monotonically. According to the Theorem 2, after the system states Z_{i1} and Z_{i2} reach the sliding mode surface $S_i = 0$, they will converge within the fixed time T_2 along sliding mode surface $S_i = 0$. Therefore, the system states Z_{i1} and Z_{i2} will be guaranteed on the sliding mode surface $S_i = 0$. In addition, even if the system states Z_{i1} and Z_{i2} is not strictly on the sliding surface $S_i = 0$, it can converge to a small region [41]. Thus, based on the analyses in cases 1 and 2, it is concluded that the system states will converge into the region W_i within fixed time T_3. Therefore, the total convergence time is bounded by $T \leq T_2 + T_3$.

According to the Theorem 1 in the [42], if $-\chi_{im}(0) < z_{i1m}(0) < \chi_{im}(0)$, $(m = u, v, r)$ and there exists a positive constant Z_M satisfying $|Z_{i1m}(t)| \leq Z_M$ for $\forall t \geq 0$, we will have $|z_{i1m}(t)| \leq \chi_{im}(t)$ for $\forall t \geq 0$. That is to say, since $\chi_{im}(t)$ is smooth and bounded, $Z_{i1m}(t)$ and $z_{i1m}(t)$ are bounded. Therefore, according to Eq. (35), (38) and (44), G_i, $\beta(Z_{i1})$ and $\tilde{\beta}(Z_{i1})$ are also bounded. Besides, since velocities w_i, w_j and w_d, are bounded, $Z_{i2m}(t)$ and $z_{i2m}(t)$ are bounded. Therefore, according to Eq. (36) and (43), B_i and $\rho(|Z_{i2}|^{r_2-1})$ is also bounded. According to the Theorem 1, The all estimation errors $\tilde{e}_{im}$, $(m = 1, 2, 3)$ are bounded, and $\hat{\Gamma}_i$ is also bounded. It follows that τ_i is bounded [43]. This completes the proof of Theorem 3.

Remark 10: By using the hyperbolic cosecant prescribed performance function and the error transformation equation, the traditional error dynamics model for the surface vessel is transferred into the prescribed performance model. It is also a simple second-order equation. Therefore, it can be utilized to design the proposed fixed-time nonsingular terminal sliding mode control scheme.

Theorem 4: : The event-triggered mechanism (46) designed can avoid the Zeno phenomenon. Moreover, the time intervals $t_{(k+1)m} - t_{km} (m = u, v, r)$ are lower bounded by a positive constant t^*.

Proof: From (46), we have

$$\left|\frac{de_{im}(t)}{dt}\right| = sign(e_{im})\dot{e}_{im} \leq |\dot{\omega}_{im}|, \quad \forall t \in [t_{km}, t_{(k+1)m}) \tag{61}$$

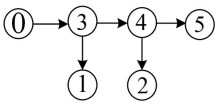

FIGURE 3. Communication topology.

where $\dot{\omega}_{im}$ is the derivative for ω_{im}, since all signals for the closed-loop system are bounded. Thus, there exists a positive constant ∇_{im} such that $|\dot{\omega}_{im}| \leq \nabla_{im}$. Because

$$e_{im}(t_{km}) = 0, \lim_{t \to t_{(k+1)m}} |e_{im}(t)| = \varsigma_{im}, \quad (m = u, v, r) \tag{62}$$

there exists the lower bound for time interval t^* and $t^* \geq \varsigma_{im}/\nabla_{im}$, Thus, the designed control law can avoid Zeno phenomenon.

V. SIMULATION RESULTS

In simulations, the model for surface vessel is used in [36]. The unknown environmental disturbances are modeled as the sum of some sinusoidal signals, and chosen as $\tau_{id} = 10 * [0.15 - 0.15cos(0.1t)cos(0.15t), 0.5 + 0.15sin(0.21t)cos(0.2t), 0.5 - 0.15sin(0.2t)cos(0.23t)]^T$. Figure 3 presents the communication topology for MSVs. It is seen that the virtual leader (the reference trajectory $\eta_d = [x_d, y_d, \psi_d]^T$ is shown in (63)) indexed by 0 and five follower vessels indexed by 1, 2, 3, 4, 5, respectively. Set the initial position and heading for each vessel as $\eta_1(0) = [-2, 0.2, 0]^T$, $\eta_2(0) = [-0.8, 1.4, 0]^T$, $\eta_3(0) = \left[0.1, 0.1, \frac{\pi}{4}\right]^T$, $\eta_4(0) = \left[2, 0, \frac{\pi}{4}\right]^T$ and $\eta_5(0) = \left[-0.8, -2, \frac{\pi}{2}\right]^T$, respectively, and set the desired deviation for MSVs as $\vartheta_1 = [1.2, 0, 0]^T$, $\vartheta_2 = [0, 1.2, 0]^T$, $\vartheta_3 = [0, 0, 0]^T$, $\vartheta_4 = [-1.2, 0, 0]^T$ and $\vartheta_5 = [0, -1.2, 0]^T$, respectively. The initial velocities $\upsilon_i(0)$ for MSVs are set as $[0, 0, 0]^T$. The simulation time is 400s and the sampling time is set to 0.01s.

$$\begin{cases} \left[\frac{t}{10}\cos(\frac{\pi}{4}), \frac{t}{10}\sin(\frac{\pi}{4}), \frac{\pi}{4}\right], & 0 \leq t < 50; \\ \left[\begin{array}{l} 5\cos(\frac{3\pi}{4} - \frac{1}{50}(t-50)) + 10\cos(\frac{\pi}{4}), \\ 5\sin(\frac{3\pi}{4} - \frac{1}{50}(t-50)), \frac{1}{50}(t-50) + \frac{\pi}{4} \end{array}\right], & 50 \leq t < 50 + 50\pi; \\ \left[\begin{array}{l} 5\cos(\frac{3\pi}{4} + \frac{1}{50}(t-50-50\pi)) + 20\cos(\frac{\pi}{4}), \\ 5\sin(\frac{3\pi}{4} + \frac{1}{50}(t-50-50\pi)) - 10\sin(\frac{\pi}{4}), \\ \frac{1}{50}(t-50-50\pi) - \frac{3\pi}{4} \end{array}\right], & 50 + 50\pi \leq t < 50 + 100\pi; \\ \left[\begin{array}{l} 25\cos(\frac{\pi}{4}) + \frac{t-50-100\pi}{10}\cos(\frac{\pi}{4}), \\ -15\sin(\frac{\pi}{4}) + \frac{t-50-100\pi}{10}\sin(\frac{\pi}{4}), \frac{\pi}{4} \end{array}\right], & t \geq 50 + 100\pi; \end{cases} \tag{63}$$

The parameters of FxESO are chosen as $\varepsilon_1 = \mu_1 = 40$, $\varepsilon_2 = \mu_2 = 150$, $\varepsilon_3 = \mu_3 = 100$, $\alpha_1 = 0.8$, $\alpha_2 = 0.6$, $\alpha_3 = 0.4$, $\beta_1 = 1.2$, $\beta_2 = 1.4$ and $\beta_3 = 1.6$, respectively. The parameters of PPF are chosen as $a_p = 0.5$, $\chi_{im0} = 0.8375$, $\chi_{im\infty} = 0.1$. The parameters for sliding mode manifold and controller are set as $r_1 = 13/11$, $r_2 = 15/13$, $r_3 = 0.7$, $r_4 = 1.8$, $\Theta = 0.1$, $\iota = 0.1$, $a_s = 2$, $b_s = 13/11$, $\alpha = \beta = 1$, $\sigma_u = 0.6$, $\sigma_v = 0.6$ and $\sigma_r = 0.15$. After all parameters are determined, the upper bound of the convergence time can be calculated as follows: $T_1 \leq 4.1s$, $T_2 \leq 12.0s$, $T_3 \leq 16.6s$, $T \leq T_2 + T_3 \leq 28.6s$.

Remark 11: From the FxESO (21), the nonlinear term $\mu_m sig^{\alpha_m}(\tilde{e}_{im})$, $0 < \alpha_m < 1$, $(m = 1, 2, 3)$ is the dominating term if estimation errors converge to near zero. And the nonlinear term $\varepsilon_m sig^{\beta_m}(\tilde{e}_{im})$, $\beta_m > 1$, $(m = 1, 2, 3)$ is the dominating term if estimation errors converge to far zero. μ_m, $(m = 1, 2, 3)$ determines the estimated performance for the FxESO. From the (19), the smaller μ_m, $(m = 1, 2, 3)$ is, the longer the convergence time is and the worse the estimated performance is. In contrast, the larger μ_m, $(m = 1, 2, 3)$ is, the shorter the convergence time is, but if it is too large, the estimated effect will oscillate. ε_1, ε_2, ε_3 are the same as μ_1, μ_2, μ_3. From the (19), α_m, $(m = 1, 2, 3)$ and β_m, $(m = 1, 2, 3)$ are also affect the convergence time. The larger α_m, $(m = 1, 2, 3)$ is, the longer the convergence time is and the worse the estimated effect is. In contrast, the smaller α_m, $(m = 1, 2, 3)$ is, the shorter the convergence time is, but if the parameter is too small, the estimation error will oscillate. The larger β_m, $(m = 1, 2, 3)$ is, the shorter the convergence time is, but if the parameter is too large, the estimated effect will oscillate. In contrast, the smaller β_m, $(m = 1, 2, 3)$ is, the longer the convergence time is and the worse the estimated effect is.

Remark 12: From the (42), the nonlinear term $\alpha sig^{r_3}(S_i)$, $0 < r_3 < 1$ is the dominating term if the S_i converge to near zero. And the nonlinear term $\beta sig^{r_4}(S_i))$, $r_4 > 1$ is dominating term if the S_i converge to far zero. α and β determines the convergence performance for the FxNTSMM. Refer to Remark 11 for the detailed parameter adjustment method.

The estimated performance for FxESO:

To show the estimated performance for FxESO, we compare it with finite-time extended state observer (FTESO) and extended state observer (ESO). The controller adopts (42) designed in this paper. The FTESO and the ESO are written as

$$\begin{cases} \dot{\hat{\eta}}_i = \hat{w}_i + \mu_1 sig^{\alpha_1}(\tilde{\eta}_i) \\ \dot{\hat{w}}_i = \hat{\Gamma}_i + \mu_2 sig^{\alpha_2}(\tilde{\eta}_i) + R_i M_i^{-1} \tau_i \\ \dot{\hat{\Gamma}}_i = \mu_3 sig^{\alpha_3}(\tilde{\eta}_i), \end{cases} \tag{64}$$

where $\mu_1 = 40$, $\mu_2 = 150$, $\mu_3 = 100$, $\alpha_1 = 0.8$, $\alpha_2 = 0.8$ and $\alpha_3 = 0.4$.

$$\begin{cases} \dot{\hat{\eta}}_i = \hat{w}_i + \mu_1 \tilde{\eta}_i \\ \dot{\hat{w}}_i = \hat{\Gamma}_i + \mu_2 \tilde{\eta}_i + R_i M_i^{-1} \tau_i \\ \dot{\hat{\Gamma}}_i = \mu_3 \tilde{\eta}_i, \end{cases} \tag{65}$$

where $\mu_1 = 40$, $\mu_2 = 150$, $\mu_3 = 100$.

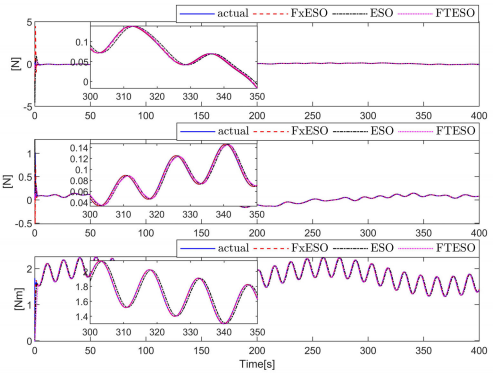

FIGURE 4. The lumped disturbances of vessel 1 and its estimations.

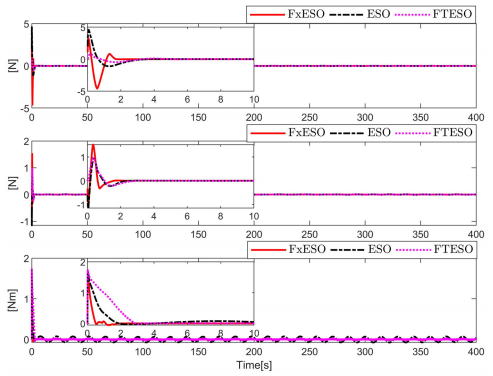

FIGURE 5. The estimation errors of lumped disturbances of vessel 1.

In this part, the vessel 1 is choose to compare the estimated performance for the three observers. Figure 4 represents the estimated effect of the three observers for lumped disturbances, where 'actual' denotes the actual lumped disturbances. The results show that the FxESO can quickly identify lumped disturbances, and the local zoom results show that the FxESO has better estimation performance than the other two observers. Figure 5 represents the estimated errors of the three observers for lumped disturbances. It is seen that compared with the other two observers, the FxESO has the fastest convergence rate and the smallest estimated errors. In addition, the convergence time of lumped disturbances estimation errors for FxESO is less than 4.1s, which verifies the validity of the proposed scheme. Figure 6 represents estimated results for the velocities. The results show that estimation performance and convergence rate for the FxESO are much better than the FTESO and the ESO. Besides, the convergence time of the velocity estimation error for FxESO is also less than 4.1s, which verifies the validity of the proposed scheme.

The controller performance for proposed control scheme:

In this part, in order to better verify the superiority for the proposed control scheme, we assume that the velocities and lumped disturbances for the surface vessels are known, and that the proposed controller has no the prescribed performance constraint and the event-triggered mechanism.

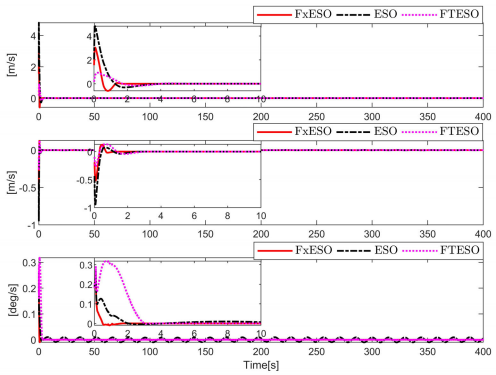

FIGURE 6. The velocity estimation error of vessel 1.

Thus, (37), (38), (42), (43) and (44) are rewritten as

$$S_i = \beta(z_{i1})z_{i1} + sig^{r_2}(z_{i2}) \tag{66}$$

$$\beta_m(z_{i1m}) = \begin{cases} (a_s|z_{i1m}|^{r_1-\frac{1}{r_2}} + b_s)^{r_2}, & |z_{i1m}| \geq \Theta \\ (a_{s1}|z_{i1m}|^{r_1-\frac{1}{r_2}} + a_{s2}|z_{i1m}|^{2-\frac{1}{r_2}} + b_s), & |z_{i1m}| < \Theta \end{cases} \tag{67}$$

$$\begin{aligned} \tau_i = -\frac{M_i R_i^{-1}}{a_{id}}[&\frac{1}{r_2}(\tilde{\beta}(z_{i1})+\beta(z_{i1}))sig^{2-r_2}(z_{i2})+a_{id}\Gamma_i \\ &- \sum_{j\in N_i} a_{ij}\dot{w}_j - a_{i0}\dot{w}_d + \frac{1}{r_2}diag\{\rho(|z_{i2}|^{r_2-1})\} \\ &\cdot diag\{|z_{i2}|^{1-r_2}\}(\alpha sig^{r_3}(S_i) + \beta sig^{r_4}(S_i))] \end{aligned} \tag{68}$$

In addition, we compare the FxNTSMM and controller proposed in this paper with the finite-time nonsingular terminal sliding mode manifold (FTNTSMM) and controller proposed in [32]. The FTNTSMM and the controller are constructed as

$$S_i = z_{i2} + k\beta(z_{i1}) \tag{69}$$

$$\beta(z_{i1}) = \begin{cases} sig^{r_1}(z_{i1}) & if\ \bar{S}_i = 0 or \bar{S}_i \neq 0,\ z_{i1} \geq \Theta \\ \kappa_1 z_{i1} + \kappa_2 sig^2(z_{i1}) & if\ \bar{S}_i \neq 0,\ z_{i1} \leq \Theta \end{cases} \tag{70}$$

$$\bar{S}_i = z_{i2} + ksig^{r_1}(z_{i1}) \tag{71}$$

$$\begin{aligned} \tau_i = -\frac{M_i R_i^{-1}}{a_{id}}[&k\dot{\beta}(z_{i1}) + k_1 S_i + k_2 sig^{r_1}(S_i) + a_{id}\Gamma_i \\ &- \sum_{j\in N_i} a_{ij}\dot{w}_j - a_{i0}\dot{w}_d] \end{aligned} \tag{72}$$

where all the parameters are the same as the [32].

Similarly, the veseel 1 is choose to compare the performance for two schemes. Figure 7 represents the simulation comparison of the initial convergence performance for the two sliding mode manifolds. It can be known that the convergence rate for the FxNTSMM is significantly faster than the FTNTSMM. Figure 8 shows the simulation comparison of the initial tracking errors for the two controllers. The results show that the proposed control scheme has faster convergence rate and smaller tracking errors.

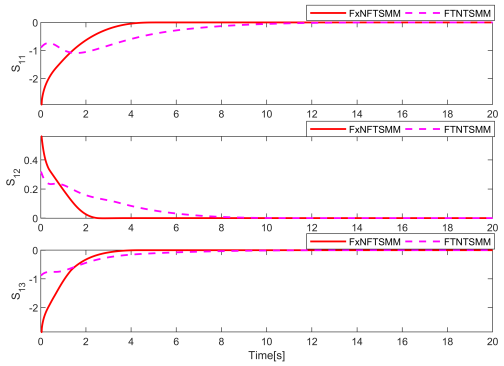

FIGURE 7. Comparisons of the initial sliding mode manifold of vessel 1.

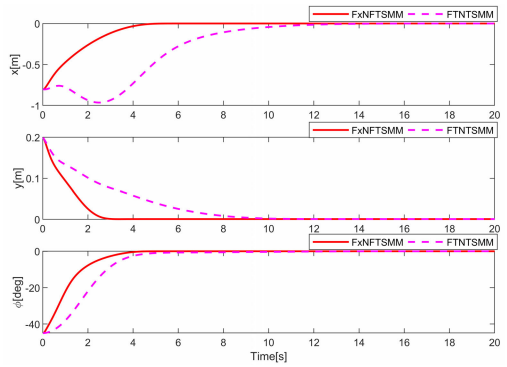

FIGURE 8. Comparisons of the initial tracking errors of vessel 1.

The simulation results for proposed controller with prescribed performance constraints:

In order to show the effectiveness of the prescribed performance constraints in this paper, we cancel the event-triggered mechanism and compare the simulation results of the proposed scheme with the prescribed performance constraints and the proposed scheme without the prescribed performance constraints. Figure 9-10 show the tracking errors of MSVs under the prescribed performance constraints and the tracking errors of MSVs without the prescribed performance constraints, respectively. It is clear that the tracking errors under the prescribed performance constraints can be constrained in the region surrounded by the prescribed performance functions and the convergence time under the prescribed performance constraints is shorter than that without the prescribed performance constraints. Figure 11-12 describe the control inputs of MSVs under the prescribed performance constraints and the control inputs of MSVs without the prescribed performance constraints, respectively.

The simulation results for proposed event-triggered controller with the prescribed performance constraints:

Figure 13 represents the event-triggered time interval of the proposed controller for the vessel 1. The horizontal axis is the triggered moment, and the vertical axis is the time interval for controller update. The length for the triggered time interval determines the update frequency for the controller. Low update frequency means less update

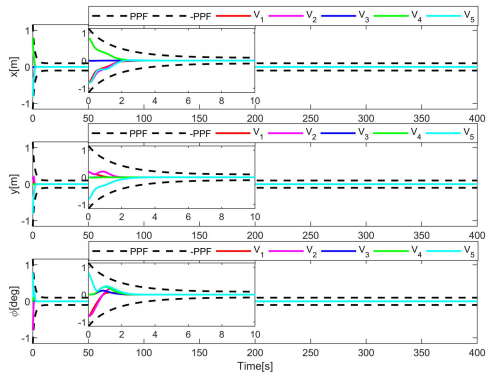

FIGURE 9. The tracking errors of MSVs under the prescribed performance constraints.

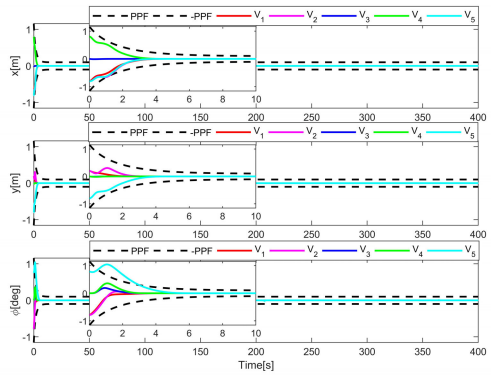

FIGURE 10. The tracking errors of MSVs without the prescribed performance constraints.

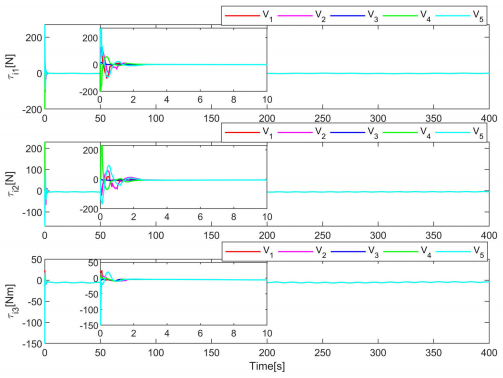

FIGURE 11. The control inputs of MSVs under the prescribed performance constraints.

TABLE 1. The comparisons of event-triggered strategy and non-event-triggered strategy.

Vessel number	Event-triggered strategy	Non-event-triggered strategy
Vessel 1	2537,2782,1532	40000,40000,40000
Vessel 2	2178,2532,1763	40000,40000,40000
Vessel 3	2472,2583,1605	40000,40000,40000
Vessel 4	2353,2753,1614	40000,40000,40000
Vessel 5	2586,2798,1856	40000,40000,40000

and communication times for the controller. To verify the effectiveness for the proposed event-triggered scheme,

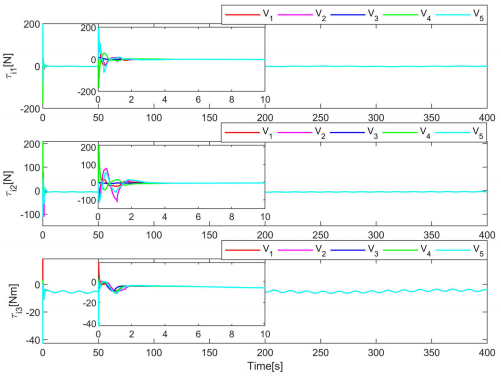

FIGURE 12. The control inputs of MSVs without the prescribed performance constraints.

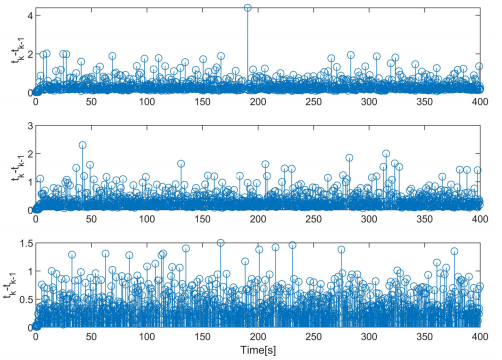

FIGURE 13. The event-triggered time interval for the control input of vessel 1.

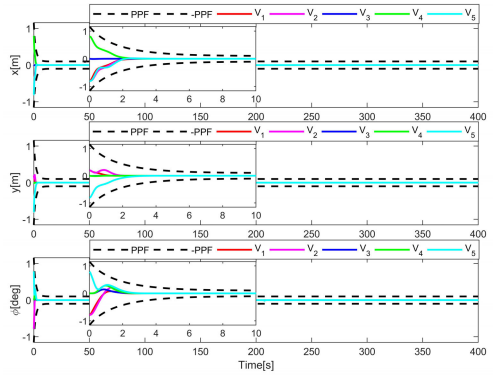

FIGURE 14. Tracking errors of MSVs with the prescribed performance constraints based on event-triggered strategy.

we compare it with non-event-triggered strategy. Table 1 denotes that the comparisons for update times of controllers with event-triggered strategy and with non-event-triggered strategy. Figure 14 shows the tracking errors of MSVs with the prescribed performance constraints based on event-triggered strategy. In addition, the convergence time of tracking errors for MSVs is less than 28.6s, which verifies the validity of the proposed scheme. By comparing with Figure 9, the results show that the introduced event-triggered scheme does not affect the tracking performance for the system. Figure 15 depicts the control inputs of MSVs with the prescribed performance constraints based on event-triggered

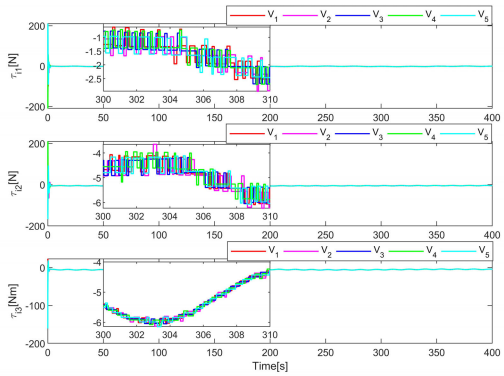

FIGURE 15. The control inputs of MSVs with the prescribed performance constraints based on event-triggered strategy.

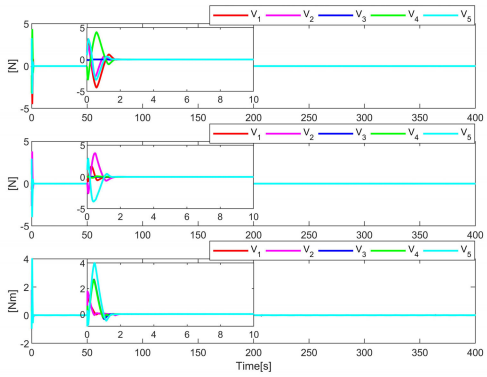

FIGURE 16. The estimation errors of MSVs of lumped disturbances.

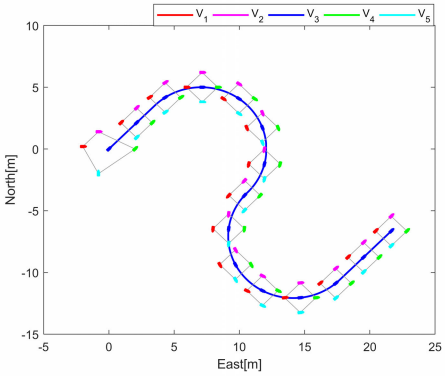

FIGURE 17. Trajectories of MSVs under cooperative control.

strategy. Figure 16 shows the estimation errors of lumped disturbances for MSVs. And figure 17 denotes the trajectories of MSVs under cooperative control based on event-triggered strategy with the prescribed performance constraints.

VI. CONCLUSION

A novel fixed-time nonsingular terminal sliding mode control method is proposed to solve the distributed cooperative control problem for MSVs. The FxESO was designed to provide the estimations of velocities and lumped disturbances. A hyperbolic cosecant prescribed performance function is incorporated into the cooperative control algorithm to improve the convergence performance of MSVs. The proposed event-triggered based on fixed-time nonsingular terminal sliding mode control scheme is applied to the cooperative control of MSVs, and the control performance is superior. Finally, simulation results of 3-DOF fully-actuated MSVs are presented to verify the effectiveness of the proposed controller. For the future work, the fixed-time sliding mode cooperative control subject to address actuator saturation and address the control problem for underactuated surface vehicles.

REFERENCES

[1] P. Mahacek, C. A. Kitts, and I. Mas, "Dynamic guarding of marine assets through cluster control of automated surface vessel fleets," *IEEE/ASME Trans. Mechatronics*, vol. 17, no. 1, pp. 65–75, Feb. 2012.

[2] G. Xia, C. Sun, B. Zhao, and J. Xue, "Cooperative control of multiple dynamic positioning vessels with input saturation based on finite-time disturbance observer," *Int. J. Control, Autom. Syst.*, vol. 17, no. 2, pp. 370–379, Feb. 2019.

[3] G. Xia, C. Sun, and B. Zhao, "Output feedback cooperative dynamic positioning control for an unactuated floating object using multiple vessels," *J. Mar. Sci. Eng.*, vol. 9, no. 5, p. 463, Apr. 2021.

[4] Z.-H. Pang, L.-Z. Fan, J. Sun, K. Liu, and G.-P. Liu, "Detection of stealthy false data injection attacks against networked control systems via active data modification," *Inf. Sci.*, vol. 546, pp. 192–205, Feb. 2021.

[5] X. He and Z. Geng, "Point stabilization and trajectory tracking of underactuated surface vessels: A geometric control approach," *J. Franklin Inst.*, vol. 358, no. 14, pp. 7119–7141, Sep. 2021.

[6] O. Elhaki and K. Shojaei, "Robust saturated dynamic surface controller design for underactuated fast surface vessels including actuator dynamics," *Ocean Eng.*, vol. 229, Jun. 2021, Art. no. 1089871.

[7] L. Cao, D. Yao, H. Li, W. Meng, and R. Lu, "Fuzzy-based dynamic event triggering formation control for nonstrict-feedback nonlinear MASs," *Fuzzy Sets Syst.*, vol. 452, pp. 1–22, Jan. 2022.

[8] Y. Huang and Y. Jia, "Fixed-time consensus tracking control for second-order multi-agent systems with bounded input uncertainties via NFFTSM," *IET Control Theory Appl.*, vol. 11, no. 16, pp. 2900–2909, Oct. 2017.

[9] N. Wang, S. Lv, M. Er, and W. Chen, "Fast and accurate trajectory tracking control of an autonomous surface vehicle with unmodeled dynamics and disturbances," *IEEE Trans. Intell. Vehicles*, vol. 1, no. 3, pp. 230–243, Sep. 2016.

[10] N. Wang, S. Lv, W. Zhang, Z. Liu, and M. J. Er, "Finite-time observer based accurate tracking control of a marine vehicle with complex unknowns," *Ocean Eng.*, vol. 145, pp. 406–415, Nov. 2017.

[11] B. Tian, Z. Zuo, X. Yan, and H. Wang, "A fixed-time output feedback control scheme for double integrator systems," *Automatica*, vol. 80, pp. 17–24, Jun. 2017.

[12] B. Tian, H. Lu, Z. Zuo, and W. Yang, "Fixed-time leader–follower output feedback consensus for second-order multiagent systems," *IEEE Trans. Cybern.*, vol. 49, no. 4, pp. 1545–1550, Apr. 2019.

[13] J. Zhang, S. Yu, D. Wu, and Y. Yan, "Nonsingular fixed-time terminal sliding mode trajectory tracking control for marine surface vessels with anti-disturbances," *Ocean Eng.*, vol. 217, Dec. 2020, Art. no. 108158.

[14] Y. Yan and S. Yu, "Sliding mode tracking control of autonomous underwater vehicles with the effect of quantization," *Ocean Eng.*, vol. 151, pp. 322–328, Mar. 2018.

[15] M. Van, M. Mavrovouniotis, and S. S. Ge, "An adaptive backstepping nonsingular fast terminal sliding mode control for robust fault tolerant control of robot manipulators," *IEEE Trans. Syst., Man, Cybern. Syst.*, vol. 49, no. 7, pp. 1448–1458, Jul. 2019.

[16] J. Mishra, C. Li, X. Yan, M. Jalili, and X. Yu, "Robust second-order consensus using a fixed-time convergent sliding surface in multiagent systems," *IEEE Trans. Cybern.*, vol. 11, no. 6, pp. 766–773, Feb. 2020.

[17] B. Zhou, B. Huang, Y. Su, Y. Zheng, and S. Zheng, "Fixed-time neural network trajectory tracking control for underactuated surface vessels," *Ocean Eng.*, vol. 236, Sep. 2021, Art. no. 109416.

[18] J. Zhang, S. Yu, and Y. Yan, "Fixed-time output feedback trajectory tracking control of marine surface vessels subject to unknown external disturbances and uncertainties," *ISA Trans.*, vol. 93, pp. 145–155, Oct. 2019.
[19] C. P. Bechlioulis and G. A. Rovithakis, "Robust adaptive control of feedback linearizable MIMO nonlinear systems with prescribed performance," *IEEE Trans. Autom. Control*, vol. 53, no. 9, pp. 2090–2099, Oct. 2008.
[20] M. Fu and L. Wang, "Adaptive finite-time event-triggered control of marine surface vehicles with prescribed performance and output constraints," *Ocean Eng.*, vol. 238, Oct. 2021, Art. no. 109712.
[21] G. Zong, Y. Wang, H. R. Karimi, and K. Shi, "Observer-based adaptive neural tracking control for a class of nonlinear systems with prescribed performance and input dead-zone constraints," *Neural Netw.*, vol. 147, pp. 126–135, Mar. 2022.
[22] G. Zong, Q. Xu, X. Zhao, S. Su, and L. Song, "Output-feedback adaptive neural network control for uncertain nonsmooth nonlinear systems with input deadzone and saturation," *IEEE Trans. Cybern.*, early access, Nov. 23, 2022, doi: 10.1109/TCYB.2022.3223351.
[23] Y. Zhang, C. Hua, and K. Li, "Disturbance observer-based fixed-time prescribed performance tracking control for robotic manipulator," *Int. J. Syst. Sci.*, vol. 50, no. 13, pp. 2437–2448, 2019.
[24] H. Liang, L. Chen, Y. Pan, and H. Lam, "Fuzzy-based robust precision consensus tracking for uncertain networked systems with cooperative-antagonistic interactions," *IEEE Trans. Fuzzy Syst.*, early access, Aug. 22, 2022, doi: 10.1109/TFUZZ.2022.3200730.
[25] L. Cao, Z. Cheng, Y. Liu, and H. Li, "Event-based adaptive NN fixed-time cooperative formation for multiagent systems," *IEEE Trans. Neural Netw. Learn. Syst.*, early access, Aug. 10, 2022, doi: 10.1109/TNNLS.2022.3210269.
[26] M. Zhao, C. Peng, W. He, and Y. Song, "Event-triggered communication for leader-following consensus of second-order multiagent systems," *IEEE Trans. Cybern.*, vol. 48, no. 6, pp. 1888–1897, Jun. 2018.
[27] Y. Deng, X. Zhang, N. Im, G. Zhang, and Q. Zhang, "Event-triggered robust fuzzy path following control for underactuated ships with input saturation," *Ocean Eng.*, vol. 186, Aug. 2019, Art. no. 106122.
[28] G. Xia, X. Xia, Z. Bo, X. Sun, and C. Sun, "Event-triggered controller design for autopilot with input saturation," *Math. Problems Eng.*, vol. 2020, pp. 1–7, Jun. 2020.
[29] G. Song, P. Shi, and R. K. Agarwal, "Fixed-time sliding mode cooperative control for multiagent networks via event-triggered strategy," *Int. J. Robust Nonlinear Control*, vol. 31, no. 1, pp. 21–36, Jan. 2021.
[30] G. Xia, C. Sun, B. Zhao, X. Xia, and X. Sun, "Neuroadaptive distributed output feedback tracking control for multiple marine surface vessels with input and output constraints," *IEEE Access*, vol. 7, pp. 123076–123085, 2019.
[31] Y. Huang and Y. Jia, "Adaptive fixed-time six-DOF tracking control for noncooperative spacecraft fly-around mission," *IEEE Trans. Control Syst. Technol.*, vol. 27, no. 4, pp. 1796–1802, Jul. 2018.
[32] K. Liang, X. Lin, Y. Chen, J. Li, and F. Ding, "Adaptive sliding mode output feedback control for dynamic positioning ships with input saturation," *Ocean Eng.*, vol. 206, Jun. 2020, Art. no. 107245.
[33] H. Sun, G. Zong, J. Cui, and K. Shi, "Fixed-time sliding mode output feedback tracking control for autonomous underwater vehicle with prescribed performance constraint," *Ocean Eng.*, vol. 247, Mar. 2022, Art. no. 110673.
[34] M. Basin, P. Yu, and Y. Shtessel, "Finite- and fixed-time differentiators utilising HOSM techniques," *IET Control Theory Appl.*, vol. 11, no. 8, pp. 1144–1152, May 2016.
[35] L. Zhang, C. Wei, R. Wu, and N. Cui, "Fixed-time extended state observer based non-singular fast terminal sliding mode control for a VTVL reusable launch vehicle," *Aerosp. Sci. Technol.*, vols. 82–83, pp. 70–79, Nov. 2018.
[36] R. Skjetne, T. I. Fossen, and P. V. Kokotović, "Adaptive maneuvering, with experiments, for a model ship in a marine control laboratory," *Automatica*, vol. 41, no. 2, pp. 289–298, Feb. 2005.
[37] G. Xia, X. Xia, B. Zhao, C. Sun, and X. Sun, "A solution to leader following of underactuated surface vessels with actuator magnitude and rate limits," *Int. J. Adapt. Control Signal Process.*, vol. 35, no. 9, pp. 1860–1878, Sep. 2021.
[38] T. Wu, H. Wang, Y. Yu, Y. Liu, and J. Wu, "Quantized fixed-time fault-tolerant attitude control for hypersonic reentry vehicles," *Appl. Math. Model.*, vol. 98, pp. 143–160, Oct. 2021.
[39] A.-M. Zhou, K. D. Kumar, Z.-G. Hou, and X. Liu, "Finite-time attitude tracking control for spacecraft using terminal sliding mode and Chebyshev neural network," *IEEE Trans. Syst., Man, Cybern. B, Cybern.*, vol. 41, no. 4, pp. 950–963, Aug. 2011.
[40] Z. Ren, T. Xia, and X. Wang, "Nonsingular terminal sliding mode-based distributed cooperative event-triggered control for multiple surface vessels under actuator faults with input saturation," *IEEE Access*, vol. 11, pp. 1115–1127, 2023.
[41] L. Zhang, S. Xu, X. Ju, and N. Cui, "Flexible satellite control via fixed-time prescribed performance control and fully adaptive component synthesis vibration suppression," *Nonlinear Dyn.*, vol. 100, no. 4, pp. 3413–3432, Jun. 2020.
[42] Y. Wang and J. Hu, "Improved prescribed performance control for air-breathing hypersonic vehicles with unknown deadzone input nonlinearity," *ISA Trans.*, vol. 79, pp. 95–107, Aug. 2018.
[43] K. Shojaei and A. Chatraei, "Robust platoon control of underactuated autonomous underwater vehicles subjected to nonlinearities, uncertainties and range and angle constraints," *Appl. Ocean Res.*, vol. 110, May 2021, Art. no. 102594.

ZHEDA REN received the bachelor's degree in electrical engineering and automation from Heilongjiang University, in 2015, and the master's degree in electronic engineering from the Harbin University of Science and Technology, in 2018. He is currently pursuing the Ph.D. degree in control science and engineering with Harbin Engineering University. His research interests include ship motion control, cooperative control, intelligent control theory, and multiagent systems.

TIAN XIA received the bachelor's degree in ship and ocean engineering from Harbin Engineering University, in 2011. He is currently pursuing the master's degree in ship and ocean engineering with Northwestern Polytechnical University. His research interest includes ship modeling and simulation and control.